



Article

Nonlinear Response of RC Columns Subjected to Equal Energy-Double Impact Loads

Warakorn Tantrapongsaton¹, Chayanon Hansapinyo^{2,*} , Suchart Limkatanyu³, Hexin Zhang⁴  and Vanissorn Vimonsatit⁵

¹ Department of Civil Engineering, Chiang Mai University, Chiang Mai 50200, Thailand

² Excellence Center in Infrastructure Technology and Transportation Engineering, Department of Civil Engineering, Chiang Mai University, Chiang Mai 50200, Thailand

³ Department of Civil Engineering, Prince of Songkla University, Songkhla 90110, Thailand

⁴ School of Engineering and the Built Environment, Edinburgh Napier University, Edinburgh, Scotland EH10 5DT, UK

⁵ School of Engineering, Macquarie University, Sydney, NSW 2113, Australia

* Correspondence: chayanon@eng.cmu.ac.th

Abstract: Defining the damage and deflection from impact by using only the impact energy could be misleading due to the effect of impact momentum. In addition, reinforced concrete columns might be subjected to repeated impact loading. Hence, this study presents the numerical simulation of 16 RC columns with identical sizing and reinforcement details, subjected to equal energy-double impact loadings using a free-falling mass at midspan. The impact energy was kept constant for both impacts. For each analysis, the impact momentum was varied by varying the velocity and mass of the impactor. The axial load ratios of the columns are between 0.0 to 0.3 of the compressive strength of the concrete cross-section. The results clearly addressed the momentum effect on the impact responses. The momentum level affected the specimens' damage behavior under the same input impact energy. A high momentum impact yielded more global flexural damage with large deflection, and a low momentum impact produced more local damage with a slight deflection. The axial load helps maintain the impact resistance capacity. However, the failure determined by the flexural damage pattern under the first impact was changed when subjected to the second impact to the shear mode with the presence of axial load. Further, the colliding index considering the momentum was used in the deflection prediction equation. The proposed equation improved the deflection calculation accuracy of reinforced concrete beams under equal energy but different momentum impact.

Keywords: concrete column; double impact; momentum; colliding index



Citation: Tantrapongsaton, W.; Hansapinyo, C.; Limkatanyu, S.; Zhang, H.; Vimonsatit, V. Nonlinear Response of RC Columns Subjected to Equal Energy-Double Impact Loads. *Buildings* **2022**, *12*, 1420. <https://doi.org/10.3390/buildings12091420>

Academic Editor: Elena Ferretti

Received: 20 August 2022

Accepted: 8 September 2022

Published: 10 September 2022

Publisher's Note: MDPI stays neutral with regard to jurisdictional claims in published maps and institutional affiliations.



Copyright: © 2022 by the authors. Licensee MDPI, Basel, Switzerland. This article is an open access article distributed under the terms and conditions of the Creative Commons Attribution (CC BY) license (<https://creativecommons.org/licenses/by/4.0/>).

1. Introduction

Throughout the service life of reinforced concrete structures, the essential RC structural members, such as the RC column, may be subjected to impact loading from an accidental situation such as a vehicle crashing, ship collision, rock falling, or explosion. Moreover, during a seismic event in a dense city central area, collisions between two adjacent buildings with inadequate separation could occur [1–5]. Those events repeat several impact loads at the exact location, causing repetitive and accumulated damages to the structure [6]. When a mass collides with the RC member, the impulse happens in a highly concise period (in a few milliseconds). The structure instantly deforms with the high loading rate before the stress wave can reach the supports. This phenomenon causes the structure to behave differently from the static loading condition. Several researchers explain that, in the early stage, the impact force is resisted by the inertia force of the structure itself [7–10]. The inertia force is generated during the time of peak impact force. As a response, the structure is suddenly deformed and an extremely high acceleration is created. The distribution of the inertia force throughout the span length translates into a much higher shear force at

the impact location compared to the shear force in the static load condition. A number of the experimental and analytical investigations of RC members under impact load reported that the failure mode of the RC member could change from flexural mode to brittle shear failure mode [11–13]. Furthermore, in an extremely high-velocity impact, such as blast loading, the failure model of the RC member reportedly shifted to fully local failure, where the concrete crushing was found at the impact location [14].

For the axially compressive loaded RC members like the RC columns, the existence of the axial load greatly affects the behavior of such members. Evidently, it has both positive and negative effects on such members under the impact load [15–17]. The presence of the axial load has an inhibitory effect on the development of the concrete cracks in the member. The impact resistance capacity and stiffness have been improved. However, the axial load leads to a more dominant local shear failure mode and a sudden collapse of the structure under a high velocity impact load.

While most of the past research has focused on the structure under a single impact load, the repeat impact load leads to a more complex failure behavior of the structure [18]. Saatic and Vecchio [11] performed multiple impact load tests on the simply supported RC beams. The result showed that the damage pattern of specimens with the same total input impact energy would not necessarily be identical. The difference in the energy dissipation of each posterior impact load led to different damage patterns and deformation of the specimens induced by the prior impact. Furthermore, Jin et al. [19] reveal that the damage caused by the initial impact determines the total damage pattern of the beam. If repetitive impact occurs in the same area, the original cracks widen. Moreover, it was found that the damage from the first impact resulted in a decrease in the strength of the beams.

Usually, the magnitude of the impact and the damage are quantified by impact energy. This is because in some research, especially in experimental testing, the dropped mass was fixed as a constant while varying the impact velocity via the dropping distance [11,16,20,21]. Thus, the change in the impact velocity results in a change in the input impact energy. Furthermore, several studies proposed the equation for predicting the maximum mid-span deflection for the RC members based on the level of the input impact energy [8,22]. However, it was discovered that using only the input impact energy to predict the impact response of such a member under the impact load is insufficient [23]. Yu and Cho [24] and Hwang et al. [25] studied different combinations of the impact mass and the impact velocity while maintaining the same level of impact energy. They discovered that the behavior of the RC members changes as the impact momentum changes. The maximum deflection increased with increasing impact momentum, and the impact force increased with decreasing impact momentum. Jin et al. [26] pointed out that the impact force was directly proportional to the impact velocity. Moreover, the crack pattern was found to be dependent on the impact momentum, where more localized damage and shear plug were found in the specimen under low impact momentum.

With the significant effect of momentum and a few studies mentioning the effect on the response of reinforced concrete members under repetitive impacts, this research aims to investigate the behavior of the RC column with different magnitudes of the axial load under repeated impact loadings. The effect of different impact momentums based on the same input kinetic energy was also investigated. The explicit finite element analysis in LS-DYNA is used to simulate the impact response of the fixed-end RC beam-columns. The impact responses, such as impact force, mid-span deflection, and energy absorption, were observed. The deflection prediction equation was proposed with the inclusion of the momentum effect in terms of the colliding index.

2. Finite Element Analysis

2.1. Study Specimen Descriptions and Test Setup

In this study, a total of 16 RC columns with an identical cross-section of $220 \times 220 \text{ mm}^2$ and a clear span length of 3000 mm were selected for investigation to represent the structural column of a typical reinforced concrete low-rise building. The reinforcement detail is shown

in Figure 1. The fixed-supports boundary condition was implemented to imitate the RC columns in an actual loading condition where both ends of the columns are fully restrained. Table 1 shows the study parameters for this study. The axial load ratio ($P/A_g f'_c$) varies from 0.0 to 0.3 (in 0.1 increments), where A_g is the gross cross-sectional area of the column concrete section, f'_c is the compressive strength of the concrete, and P is the axial force of 188.57, 377.15, and 565.72 kN for axial load ratios of 0.1, 0.2, and 0.3, respectively. While each column specimen was impacted two times at mid-span with the constant level of the impact energy of 1029 J for each blow, the impact momentum varied between 1112, 786, 556, and 393 N-s based on a different combination of the impact velocity and the dropped mass. For the material, the compressive strength of the concrete material was 40 MPa. The yield strengths of DB20 bars were 500 MPa, and the RB6 bars were 318 MPa. The shear stirrups spacing arrangement were designed based on ACI 318-19 [27] for static loading (@100 mm along mid-span) and for earthquake resistance (@50 mm at the edge of the column). As per ACI 318-19 [27], the static ultimate point loads at midspan, corresponding to the static bending capacity (P_{ub}) and the static shear capacity (P_{uv}) of the samples, were calculated and illustrated in Table 2 (data from Tantrapongsaton et al. [23]). The equation for calculating the shear capacity of the RC member (V_n) subjected to axial loading based on ACI 318-19 [27] is shown below.

$$V_n = V_c + V_s \quad (1)$$

where V_c is the shear strength provided by the concrete (N), and V_s is the shear strength (N) provided by the shear reinforcements.

$$V_c = \left(0.17 \sqrt{f'_c} + \frac{N_u}{6A_g} \right) b_w d \quad (2)$$

$$V_s = \frac{A_v f_{yt} d}{s} \quad (3)$$

The N_u is the axial load (N), b_w is the width of the column (mm), d is the effective depth (mm), A_v is the sectional area of the shear reinforcement (mm^2), f_{yt} is the yield strength of the steel bar (MPa), and s is the stirrup spacing distance (mm).

The bending moment capacity of the RC column was calculated by constructing the moment-axial load interaction diagram, where the moment capacity was determined based on the axial load level of the cross-section. In general, the increase in the axial load level results in more bending moment capacity due to the additional contribution of the compression force on the column section negating the tension force created by the bending moment. The specimen nomenclature is based on the axial load ratios and the impact momentum. For example, in specimen C-0.2-1112, “0.2” refers to “0.2 axial load ratio”, and “1112” refers to the impact momentum of 1112 kg·/s.

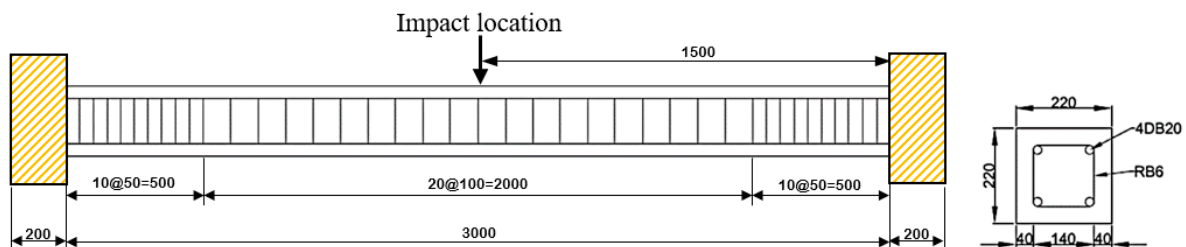


Figure 1. Cross-section and reinforcing detail of the RC specimens (unit: mm).

Table 1. Study parameter for the RC column specimens.

| Specimen | Axial Load Ratio ($P/A_g f_c'$) | Dropped Mass (kg) | Velocity (m/s) | Momentum (kg·m/s) | Impact Energy, E_k (J) |
|------------|--------------------------------------|----------------------|-------------------|----------------------|-----------------------------|
| C-0.0-1112 | 0.0 | 600 | 1.85 | 1112 * | 1029 * |
| C-0.0-786 | | 300 | 2.62 | 786 * | |
| C-0.0-556 | | 150 | 3.71 | 556 * | |
| C-0.0-393 | | 75 | 5.24 | 393 * | |
| C-0.1-1112 | 0.1 | 600 | 1.85 | 1112 * | 1029 * |
| C-0.1-786 | | 300 | 2.62 | 786 * | |
| C-0.1-556 | | 150 | 3.71 | 556 * | |
| C-0.1-393 | | 75 | 5.24 | 393 * | |
| C-0.2-1112 | 0.2 | 600 | 1.85 | 1112 * | 1029 * |
| C-0.2-786 | | 300 | 2.62 | 786 * | |
| C-0.2-556 | | 150 | 3.71 | 556 * | |
| C-0.2-393 | | 75 | 5.24 | 393 * | |
| C-0.3-1112 | 0.3 | 600 | 1.85 | 1112 * | 1029 * |
| C-0.3-786 | | 300 | 2.62 | 786 * | |
| C-0.3-556 | | 150 | 3.71 | 556 * | |
| C-0.3-393 | | 75 | 5.24 | 393 * | |

Note: “*” represents the value per single impact load.

Table 2. Calculated static capacities of the samples [23].

| Axial Load Ratio | Static Bending Capacity P_{ub} (kN) | Static Shear Capacity P_{uv} (kN) | Capacity Ratio (P_{uv}/P_{ub}) |
|------------------|--|--|---------------------------------------|
| 0.0 | 158.7 | 148.0 | 0.93 |
| 0.1 | 179.7 | 170.0 | 0.95 |
| 0.2 | 200.5 | 192.0 | 0.96 |
| 0.3 | 220.8 | 214.0 | 0.97 |

2.2. Finite Element Model

The 3D finite element model generated in the LS-DYNA [28] program was implemented to simulate the behavior of the RC columns under double impact loading. The explicit solver in LS-DYNA was selected due to its compatibility with the impact problem.

2.2.1. Structural Modeling

The main structural components of the RC column, e.g., concrete, the steel supports, and the steel hammer were modeled by using the eight-node solid hexahedron element [29,30]. Additionally, the 2×2 Gauss quadrature 2-node Huges–Lin beam element [31,32] was used to model the reinforcing steel bars, shear stirrups, and prestressing wire. The “shared node” concept in the discrete model was applied to simulate the “fully bounded” interaction between the concrete and the reinforcements (see Figure 2). The contact between two surfaces, such as concrete to support or concrete to hammer, was controlled by using the contact algorithm called “CONTACT AUTOMATIC SURFACE TO SURFACE.” The boundary condition of the test setup was simulated by using the keyword “*BOUNDARY_SPC_NODE”. This allows the user to define imposed motion on the boundary node, e.g., movement in the x, y, and z axes, and rotation around the x, y, and z axes. In this study, the boundary conditions of the specimen’s support resemble the fixed- end supports by fixing all movement and rotation about all axes. The mesh size of 20 mm was employed for all elements to balance the accuracy of the numerical results and computational time. Moreover, to simulate the acceleration of the free-falling weight, the keyword “LOAD BODY” was used to quantify the acceleration created by gravity.

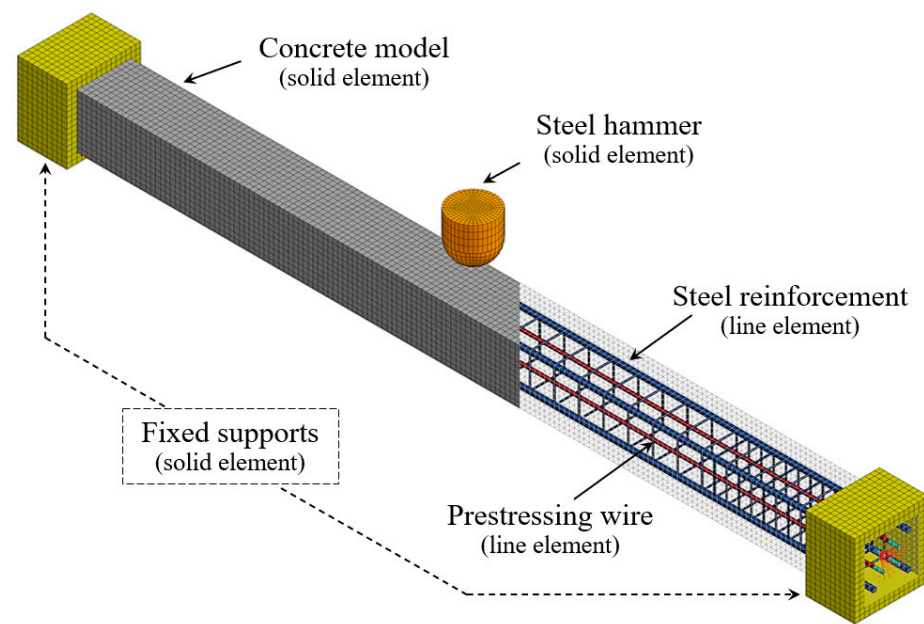


Figure 2. Cross-section and reinforcing detail of the RC specimens (unit: mm).

2.2.2. Material Modeling

Table 3 summarizes the detail of the material model used in this study. The mentioned material models were evidently used in research and were verified against the experimental results [7,8,33,34], which proved that these material models were able to simulate the behavior of the RC members under impact load effectively.

Table 3. Nonlinear material models used in the simulation.

| Segment | Material Model | Parameter | Value |
|-------------------|--|--------------------------|------------------------|
| Concrete | *MAT_CONCRETE_DAMAGE_REL3 (*MAT_072R3) | Density | 2400 kg/m ³ |
| | | Compressive strength | 40.0 MPa |
| Reinforcement | *MAT_PIECEWISE_LINEAR_PLASTICITY (*MAT_024) | Density | 7850 kg/m ³ |
| | | Young's modulus | 200 GPa |
| | | Poisson's ratio | 0.3 |
| | | Tangent modulus | 2 GPa |
| | | Yield strength (Rebar) | 500 MPa |
| | | Yield strength (Stirrup) | 318 MPa |
| Prestressing wire | *MAT_ELASTIC (*MAT_001) | Density | 7850 kg/m ³ |
| | | Young's modulus | 167 GPa |
| | | Poisson's ratio | 0.3 |
| Guiding cable | *MAT_NULL (*MAT_009) | Density | 7850 kg/m ³ |
| | | Young's modulus | 167 GPa |
| | | Poisson's ratio | 0.001 |
| Thermal element | *MAT_ELASTIC_PLASTIC_THERMAL (*MAT_004) | Density | 7850 kg/m ³ |
| | | Young's modulus | 200 GPa |
| | | Poisson's ratio | 0.3 |
| | | CTE | 0.001 |
| Hammer | *MAT_RIGID (*MAT_020) | Young's modulus | 200 GPa |
| | | Poisson's ratio | 0.3 |
| Supports | *MAT_RIGID (*MAT_020) | Young's modulus | 200 GPa |
| | | Poisson's ratio | 0.3 |

2.2.3. Strain Rate Effect

To consider the effect of the strain rate. The tensile dynamic increase factor (TDIF) proposed by Malvar and Ross [35] was used in the finite element model, as expressed in Equations (4) and (5):

$$\text{TDIF} = \frac{f_t}{f_{ts}} = \left(\frac{\dot{\epsilon}}{\dot{\epsilon}_{ts}} \right)^\delta \quad \text{for } \dot{\epsilon} \leq 1s^{-1} \quad (4)$$

$$\text{TDIF} = \frac{f_t}{f_{ts}} = \beta \left(\frac{\dot{\epsilon}}{\dot{\epsilon}_{ts}} \right)^{1/3} \quad \text{for } \dot{\epsilon} > 1s^{-1} \quad (5)$$

where f_t is dynamic tensile strength at the strain rate $\dot{\epsilon}$ in the range of 10^{-6} – $160 s^{-1}$, f_{ts} is the static tensile strength at the strain rate $\dot{\epsilon}_{ts} = 3 \times 10^{-6}$, $\log \beta = 6\delta - 2$, $\delta = 1/(1 + 8f'_c/f'_{co})$, f'_c is the static uniaxial compressive strength of concrete (in MPa), and f'_{co} is taken as 10 MPa. Based on the CEB recommendation [36], the equations of the compression dynamic increase factor (CDIF) can be expressed as Equations (6) and (7):

$$\text{CDIF} = \frac{f_c}{f_{cs}} = \left(\frac{\dot{\epsilon}}{\dot{\epsilon}_{cs}} \right)^{1.026\alpha} \quad \text{for } \dot{\epsilon} \leq 30s^{-1} \quad (6)$$

$$\text{CDIF} = \frac{f_c}{f_{cs}} = \gamma(\dot{\epsilon})^{1/3} \quad \text{for } \dot{\epsilon} > 30s^{-1} \quad (7)$$

where f_c is the dynamic compressive strength at the strain rate $\dot{\epsilon}$, f_{cs} is the static compressive strength (in MPa) at the strain rate $\dot{\epsilon}_{cs}$; $\log \gamma = 6.156\alpha - 0.49$, and $\alpha = 1/(5 + 3f_{cu}/4)$, where f_{cu} is the static cube compressive strength of concrete (in MPa). The DIF for reinforcement proposed by Malvar [37] was used as expressed in Equation (8):

$$\text{DIF} = \left(\frac{\dot{\epsilon}}{10^{-4}} \right)^\alpha \quad (8)$$

where $\alpha = 0.074 - 0.04f_y/414$, and f_y is the yield strength of the steel (in MPa).

2.2.4. The Creation of Axial Load in the RC Column Specimens

The creation of the axial load in the column specimen was carried out by implementing a complex FE-modelling technique using a “thermal element” and a “guiding cable” to simulate the post-tensioning process. This technique was originally introduced in the research of Johansson and Fredberg [38] and was utilized and fully explained in Tantrapongsaton et al. [23]. This concept resembles the process of concrete post-tensioning by placing the prestressing wire inside the guiding cable at the centroid of the column section. The prestressing wire was pulled by the thermal element attached at both ends of the prestressing wire, which shrank under negative temperature. The tension force in the prestressing wire is translated into the axial load in the column section via the anchoring plates at the column ends. The coefficient of thermal expansion used for the thermal element was equal to 0.001. The negative temperature gradients of -160 , -320 , and -500 °C were assigned to achieve 0.1, 0.2, and 0.3 axial load ratios, respectively.

2.2.5. Modelling of RC Columns under Double Impact Loading

The residual damage from the first impact must be appropriately considered when studying the effect of the RC column under double impact loading. To filter out the vibration effect in the specimen after the impact and to remove the waiting time for the specimen to return to its “still condition” before applying the subsequent impact load, each impact model (1st impact and 2nd impact) was analyzed separately. The first impact was analyzed, and the damage to the concrete and the reinforcement from the first impact model was imported to the second model by using the commands called “*INTERFACE SPRINGBACK LSDYNA” and “*INCLUDE”. The first command creates an output file

named “dynain” at the end of the simulation. This file contains the coordinates for all nodes and the maximum effective stress and strain of each element on the selected parts at the end of the simulation (in this case, the concrete and steel elements). Later, under the second impact model, the output file was included in the simulation as the initial condition for the RC column specimens via the *INCLUDE command.

3. Numerical Results and Discussions

3.1. Impact Responses

In this study, the impact momentum varied based on equal input impact energy, as stated in Section 2. As seen in Table 1, the low-impact momentum indicates a low mass–high velocity impact, and the high-impact momentum indicates a high mass–low velocity impact. The peak impact force, peak mid-span deflection, impulse, and absorbed energy are tabulated in Table 4. The peak impact force was recorded as the maximum force in an early stage of the time history curve (around 1–5 ms). During this stage, the impact force was resisted by the inertia force of the member itself, while mid-span deflection remains close to zero [7–10]. Figure 3 shows the impact behavior of the RC column under different levels of impact momentum. The low-momentum impact yields a higher peak impact force and shorter impact duration, and the high-impact momentum yields a lower peak impact force and longer impact duration. On the other hand, the mid-span deflection reaches its peak during the later stage of the impact, then enters the free vibrating stage, and finally rests in the static stage [22,23].

Table 4. Numerical results.

| Specimen | Colliding Index (E_k/p) | Peak Impact Force (kN) | | Peak Mid-Span Deflection (mm) | | Absorbed Energy (J) | |
|------------|-----------------------------|------------------------|------------|-------------------------------|------------|---------------------|------------|
| | | 1st Impact | 2nd Impact | 1st Impact | 2nd Impact | 1st Impact | 2nd Impact |
| C-0.0-1112 | 0.93 | 124.24 | 57.87 | 19.39 | 37.27 | 881 | 956 |
| C-0.0-786 | 1.31 | 165.71 | 59.98 | 16.23 | 31.93 | 740 | 821 |
| C-0.0-556 | 1.85 | 212.44 | 83.61 | 13.64 | 26.43 | 624 | 734 |
| C-0.0-393 | 2.62 | 246.09 | 95.33 | 10.46 | 20.64 | 478 | 625 |
| C-0.1-1112 | 0.93 | 141.41 | 67.16 | 15.49 | 25.73 | 814 | 879 |
| C-0.1-786 | 1.31 | 186.14 | 101.29 | 13.85 | 22.85 | 696 | 789 |
| C-0.1-556 | 1.85 | 224.17 | 125.93 | 11.28 | 19.18 | 546 | 698 |
| C-0.1-393 | 2.62 | 257.87 | 182.96 | 8.97 | 14.91 | 350 | 571 |
| C-0.2-1112 | 0.93 | 142.82 | 67.59 | 13.63 | 21.27 | 788 | 862 |
| C-0.2-786 | 1.31 | 187.33 | 132.57 | 12.09 | 20.43 | 673 | 707 |
| C-0.2-556 | 1.85 | 221.96 | 166.31 | 9.97 | 18.31 | 511 | 608 |
| C-0.2-393 | 2.62 | 261.96 | 210.55 | 8.28 | 12.98 | 325 | 476 |
| C-0.3-1112 | 0.93 | 140.52 | 97.96 | 13.03 | 18.92 | 787 | 811 |
| C-0.3-786 | 1.31 | 188.63 | 136.91 | 11.64 | 15.62 | 669 | 652 |
| C-0.3-556 | 1.85 | 224.00 | 161.02 | 9.58 | 16.53 | 505 | 520 |
| C-0.3-393 | 2.62 | 263.82 | 206.77 | 8.17 | 14.48 | 321 | 545 |

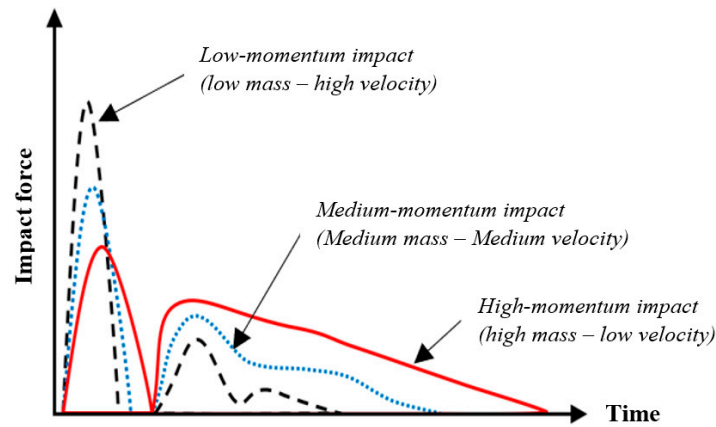


Figure 3. Impact force-time history curve of a RC column under high, medium, and low impact momentum.

3.2. Damage Pattern

From the numerical results, the damage pattern can be indicated by the effective plastic strain distribution pattern on the surface of the RC column specimens. Figure 4 shows the damage pattern of the RC column specimens under the first impact and the second impacts. From the calculated capacity ratio of about 1.0 illustrated in Table 2, the flexural-shear damage pattern was expected. The numerical results showed that all the column specimens suffered flexural cracks. It should be noted that decreasing the impact momentum results in the local damage clustering near the impact location, while increasing the impact momentum results in the global damage spreading throughout the span, indicating more global damage.

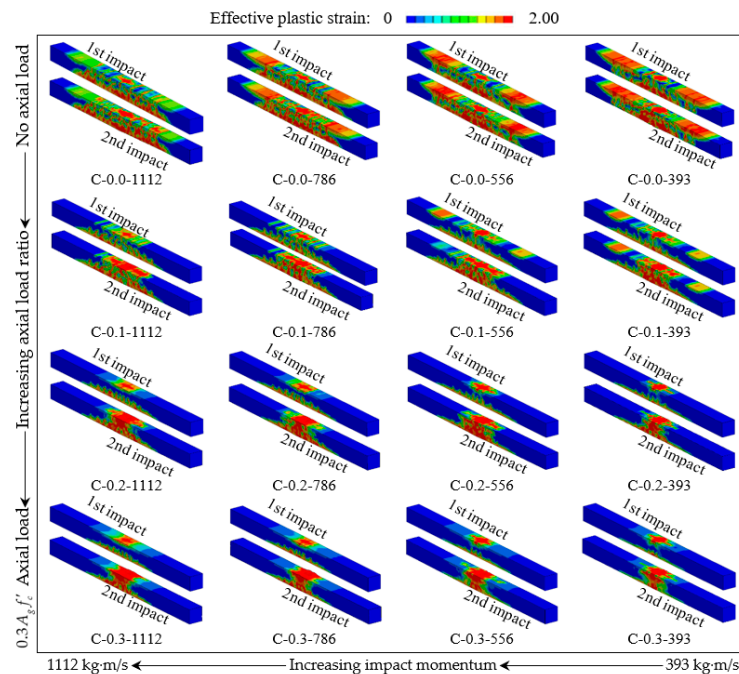


Figure 4. Damage pattern of RC column specimens under double impact loads.

Taking the specimens without axial load to consider the momentum effect, as seen in Figure 5, shows that the cracks propagated vertically from the top and bottom of the column to the mid-depth level. These flexural cracks cover almost the entire column span. The existing flexural cracks from the first impact were enlarged by the second impact, leaving more severe flexural damage to the RC columns. It should be noted that in the

specimens with lower momentum (C-0.0-556 and C-0.0-393), the flexural cracks were found more concentrated in the mid-span zone. The damage behavior is the effect of the low-momentum impact that makes the damage more localized on the impact location, as explained by Jin et al. [26].

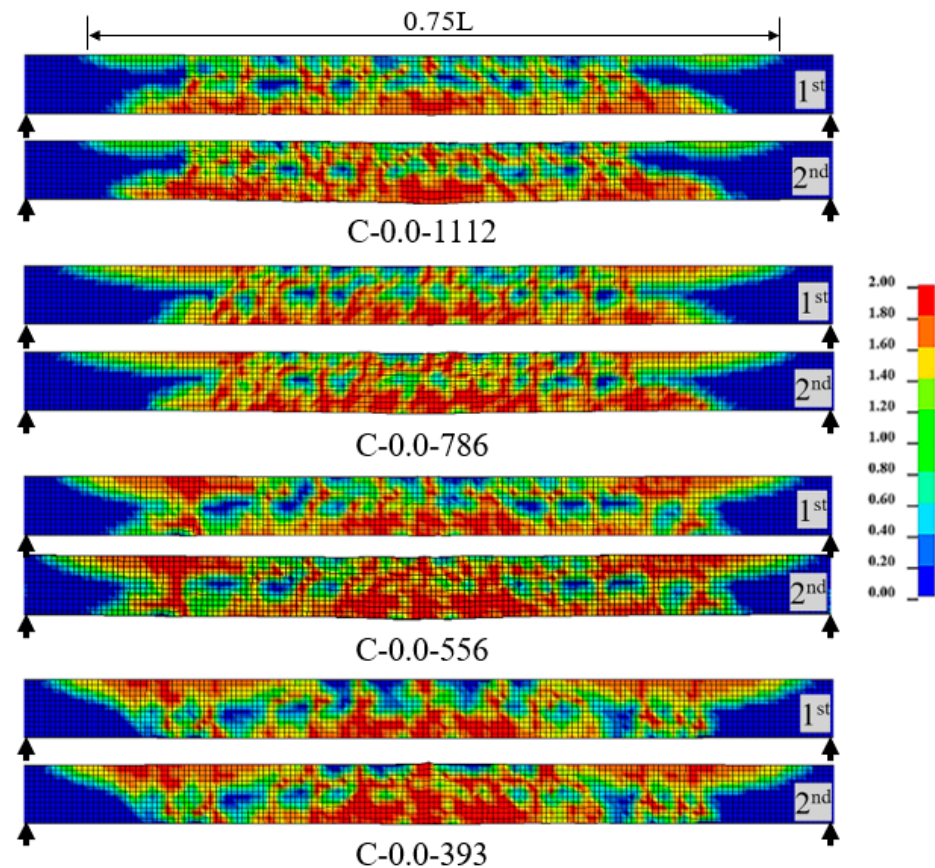


Figure 5. Damage (plastic strain) pattern of the specimen without axial load.

Usually, the failure mode of the RC members under repeated impact loading at the same location should be determined by the damage pattern from the very first impact [19]. However, the findings in this research showed that this theory only applies to a specimen without axial load. Regardless of the inhibitory effect on flexural crack development from the influence of the axial load, a new damage pattern was found in the specimen with axial load under the second impact. Figure 6 shows that under the second impact, the new shear crack developed from the existing flexural crack for the specimen with a 0.1 and 0.2 axial load ratio (C-0.1 and C-0.2). In addition, for the specimen with a 0.3 axial load ratio, the shear crack clustered even more towards the mid-span, and the concrete crushing damage was found at the impact location. This indicates that the failure model can still change from flexural mode to shear or crushing mode depending on the level of the axial load ratio, as shown in Figure 7. This is because the axial load could effectively maintain the flexural resistance of the section as long as the specimen's sections could still generate the internal compression–tension couple bending moment. However, the reformed shear damage under the second impact was due to the first impact's flexural crack, which reduced the shear transfer capacity of the concrete section.

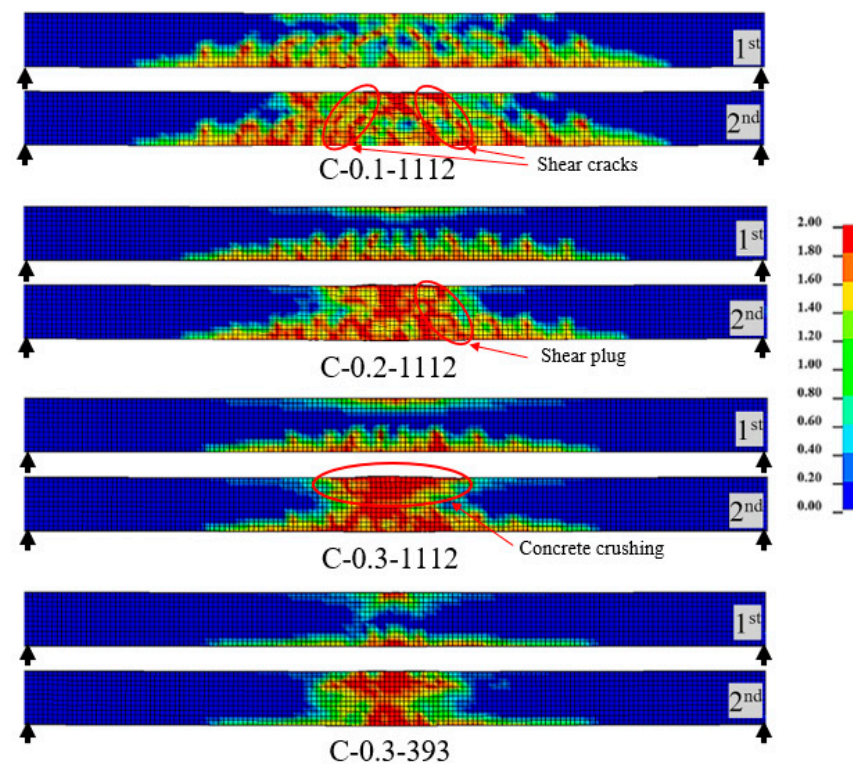


Figure 6. Damage (plastic strain) pattern of the specimens with different axial load ratios.

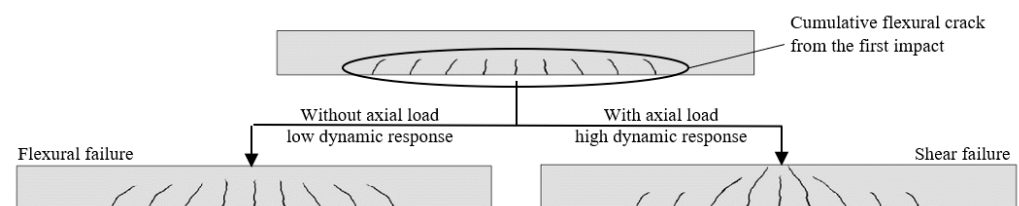


Figure 7. Change in failure mode due to the existing damage.

3.3. Effect of the Impact Momentum

Under the same input kinetic energy, the effects of the different impact momenta on the impact responses of the RC columns can be seen in Figure 8. Figure 8a shows that the impact force decreases with the increased impact momentum, both in the first and second impacts. This decrease in the peak impact force is directly related to the decrease in the impact velocity [26]. Additionally, the increases in the impact force were the effect of the strain rate of the concrete material, where the material response under high strain rate yields significantly higher stress. Under the same momentum, the peak impact force in the second impact is reduced by around 30% from that of the first impact. This is due to the residual damage caused by the first impact reducing the impact capacity of the column specimens, resulting in decreased peak impact force under the second impact.

Figure 8b shows the relationship between the peak mid-span deflection and the impact momentum. It is seen that the mid-span deflection increases with the increase of momentum. This is because the specimens were globally damaged under high momentum impact, resulting in a larger mid-span deflection in the later stationary stage. On the contrary, a relatively smaller deflection was found in the specimens under the low-momentum impact causing local damage in the early high dynamic stage.

The absorbed energy, the area under the impact force-mid-span deflection curve, has the same increasing trend as that of the peak mid-span deflection. As shown in Figure 8c, the absorbed energy increases with the increased momentum. The specimens under a high momentum impact absorbed around 75% to 90% of the input kinetic energy of 1029 J, and

the specimens under a low momentum impact absorbed only 30% to 50% of the input energy. This is because the low impact momentum specimens yielded a mid-span deflection smaller than that of the high momentum impact specimens.

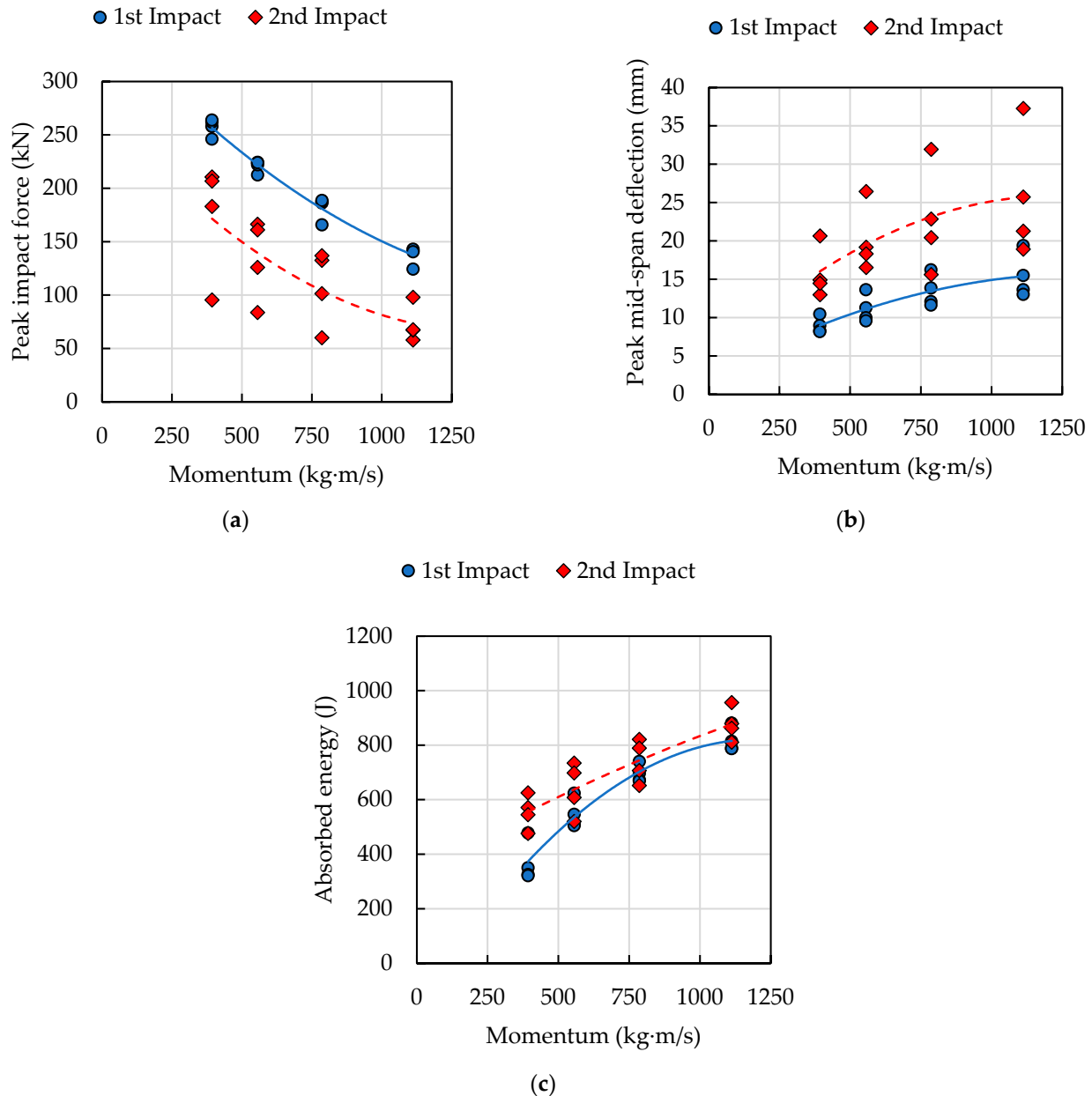


Figure 8. Relationship between the impact momentum and: (a) impact force; (b) mid-span deflection; (c) absorbed energy.

3.4. Effect of Axial Load

The axial load plays an important role in controlling the impact behavior of the RC column [13,15,16]. Figure 9 shows the second-first peak impact ratio for each axial load ratio. It was found that the specimen without axial load could only maintain around 40% (0.4 second-first impact ratio) of its impact capacity. In comparison, the specimens with 0.2 and 0.3 axial load ratios maintain around 75% (0.75 second-first impact ratio) of their impact capacity. This is due to the inhibitory effect on the concrete crack development shown in Section 3.2. However, in the case of the specimen under a large impact momentum (1112 kg·m/s), the axial load effect was minimized.

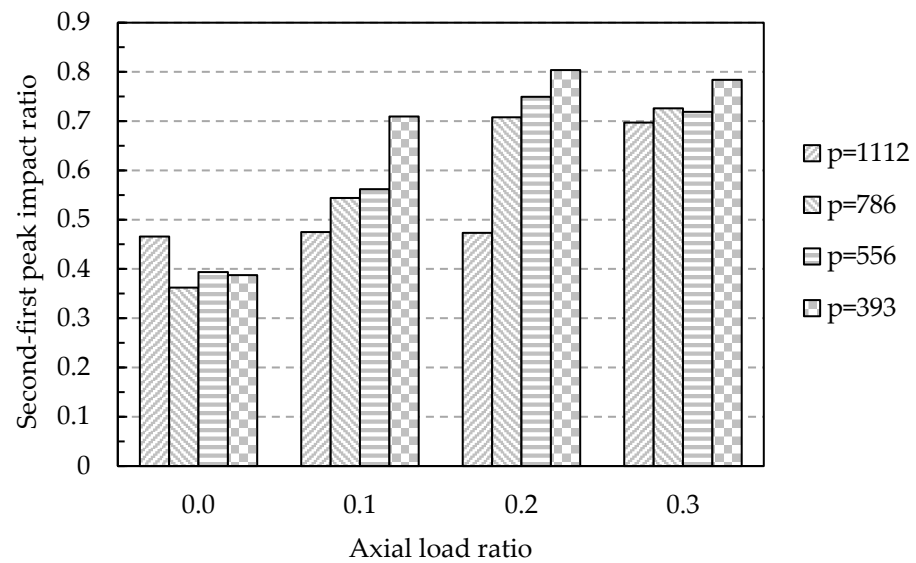


Figure 9. Second-first peak impact ratio for each axial load ratio.

For the peak mid-span deflection, the axial load also reduces the deflection of the RC columns under both first and second impact, as illustrated in Figure 10. Compared with specimens without axial load (C-0.0) as a baseline, the specimens with axial load ratios of 0.1, 0.2, and 0.3 yield approximately 12%, 27%, and 41% less mid-span deflection, respectively. This number applies to both the first and the second impacts.

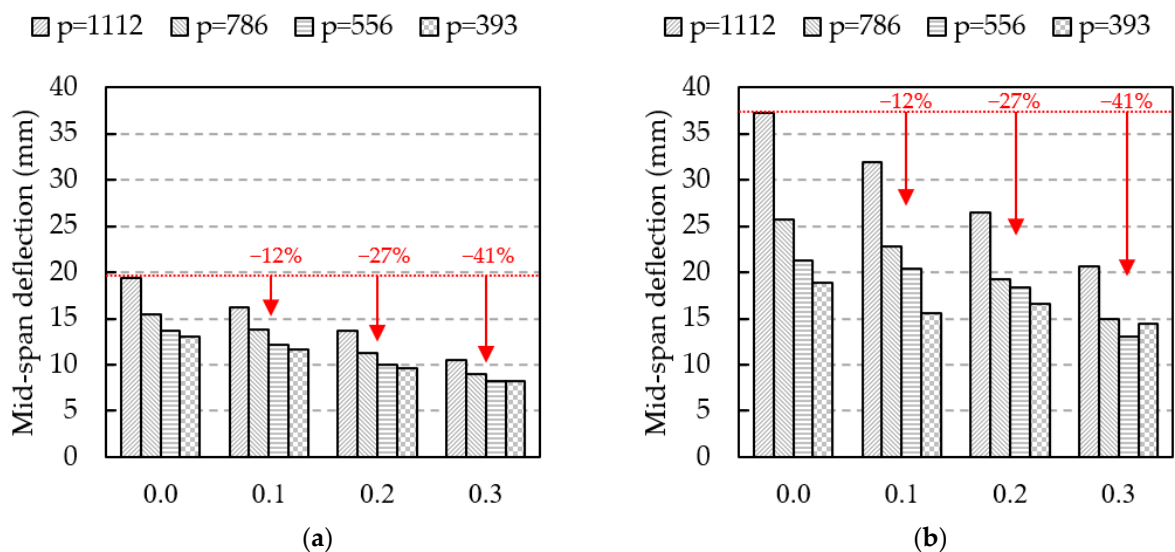


Figure 10. Relationships between mid-span deflection and axial load ratio of RC column specimen under: (a) first impact; (b) second impact.

3.5. Distribution of the Internal Forces

In the early stage of the impact load, the acceleration of the RC column creates an inertia force in the opposite direction of the impact load with a magnitude equal to mass times acceleration integrated over the volume [7–10].

Figure 11a,b show the distribution of the acceleration (inertial per unit mass of the column length) during the peak time of impact force at the column mid-span of the specimens with different axial ratios (0.0, 0.2, and 0.3) under the first and second impacts, respectively. It is seen that the peak acceleration occurring around the mid-span is increased with the increase in axial load level. In addition, specimen C-0.3 (0.3 axial load ratio) shows

a unique shape of the peak acceleration distribution curve, having positive acceleration values next to the column mid-span (see Figure 11a). However, the positive acceleration disappeared after the RC column was subjected to the second impact (see Figure 11b). Later, the inertia force was found to be significantly decreased when the specimen was subjected to the second impact. This is because of the loss in the global stiffness of the damaged column section due to the first impact.

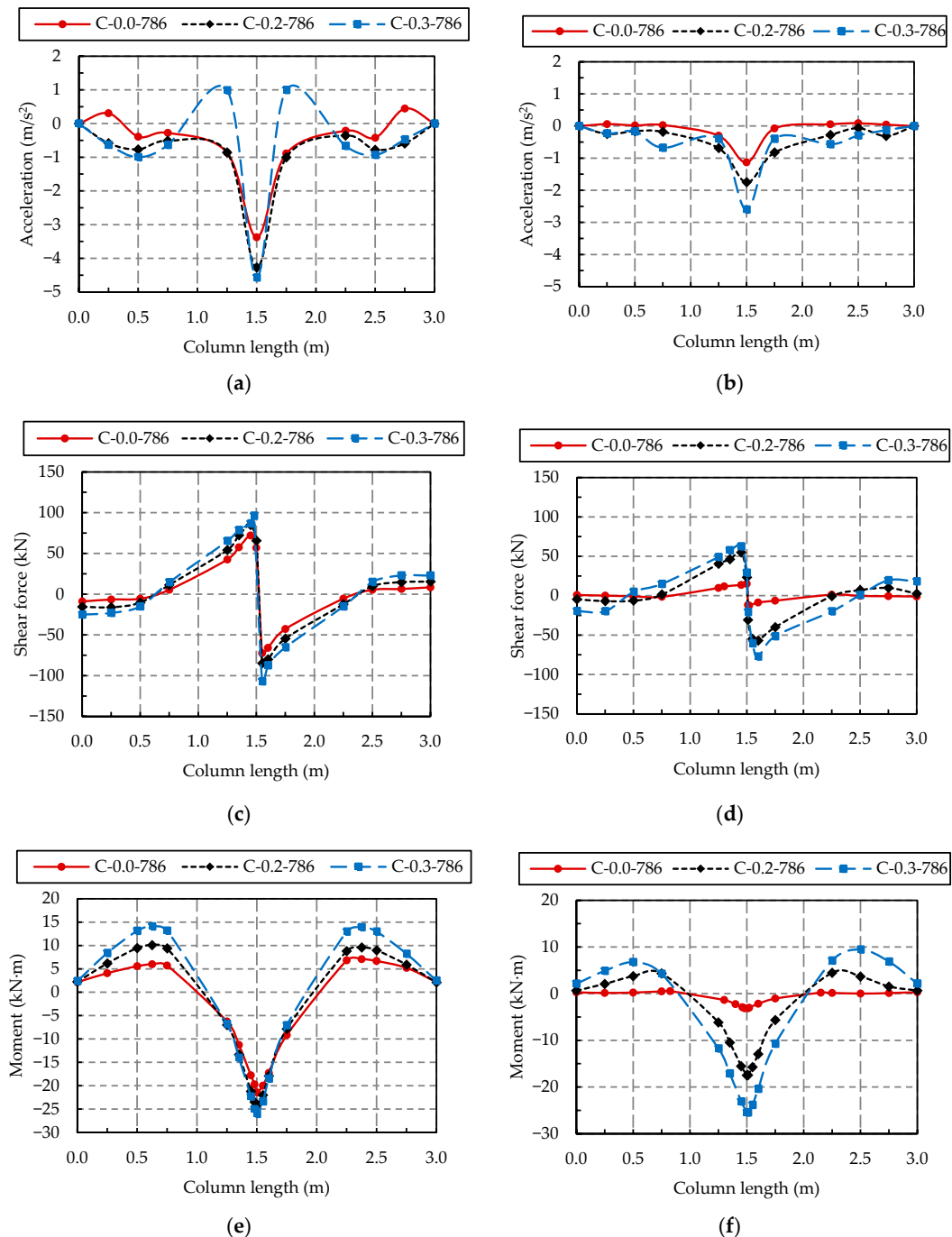


Figure 11. (a) Acceleration at the time of peak impact force under the first impact load. (b) Acceleration at the time of peak impact force under the second impact load. (c) Shear force at the time of peak impact force under the first impact load. (d) Shear force at the time of peak impact force under the second impact load. (e) Moment at the time of peak impact force under the first impact load. (f) Moment at the time of peak impact force under the second impact load.

Figure 11c,d show the shear force distribution of the RC columns under impact load at the peak impact force time. It is seen that the shear force increases with the increased axial load level. The shape of the shear force distribution curve shows that the RC column was subjected to the highest shear force near the impact location. Figure 11d shows that under the second impact load, the specimens with axial load (C-0.2 and C-0.3) were still able to maintain around 64% of the original shear force from the first impact load, while the specimen without axial load lost over 80% of its shear force under the second impact, which is directly related to the loss in peak impact force shown in Figure 9. This relatively high shear force within the specimens with axial load (C-0.2 and C-0.3) led to the change in failure mode from flexural mode to shear failure mode.

Lastly, the moment distribution at the time of peak impact force of the RC columns under the first and second impact is shown in Figure 11e,f. It was observed that the moment increased with the increase in axial load level. Even though only minor differences in the moments were shown in Figure 11e, Figure 11f shows a significant effect of axial load on the moment capacity of the RC column under the second impact load. It is seen that the specimen without axial load lost almost 85% of the moment from the first impact, while the specimen with a 0.2 axial load ratio lost only 27% of the moment from the first impact. Nevertheless, after the axial load ratio increases to 0.3, the moment capacity of specimen C-0.3 remains the same as the first impact.

Thus, this internal force distribution confirms that the axial load level has a significant effect on the shear and moment resistance of the RC column, which leads to the change in the overall failure mode of the RC column from global flexural failure to local shear failure.

3.6. Colliding Index in Deflection Prediction

Several studies have employed the input kinetic energy to describe the magnitude of the impact action on the RC members. However, using kinetic energy alone can be misleading since the impact loading is instantaneous. The impact response of the RC member changes with the strain rate [11,39,40]. Section 3.2 shows the different failure modes of the equal energy impacted specimens. To indicate the level of the collision, the colliding index (*CI*), which is the ratio of the impact energy to the impact momentum, as expressed in Equation (9), was used [23]. The high-velocity impact with a lighter dropped mass can be referred to as a high level of colliding index, and the low-velocity impact with a heavier dropped mass can be referred to as a low level of the colliding index.

$$CI = \frac{E_k}{p} = \frac{\frac{1}{2}mv^2}{mv} \quad (9)$$

Figure 12 shows the relationship of the colliding index with the impact force and the mid-span deflection under equal impact energy. It was evident that the impact force was increased proportionally to the increasing colliding index for the specimens under the first impact. This agrees well with the Jin et al. [26] research, where the impact force was found to be directly proportional to the impact velocity. On the other hand, it was found that the mid-span deflection is significantly larger when subjected to a small colliding index based on the same input kinetic energy. It should be noted that the variation in the values of the mid-span deflection of the specimen under the same colliding index indicated the effect of the axial load, where a significant difference in mid-span deflection was found on the specimen under a lower colliding index (less than 1.0) in the second impact.

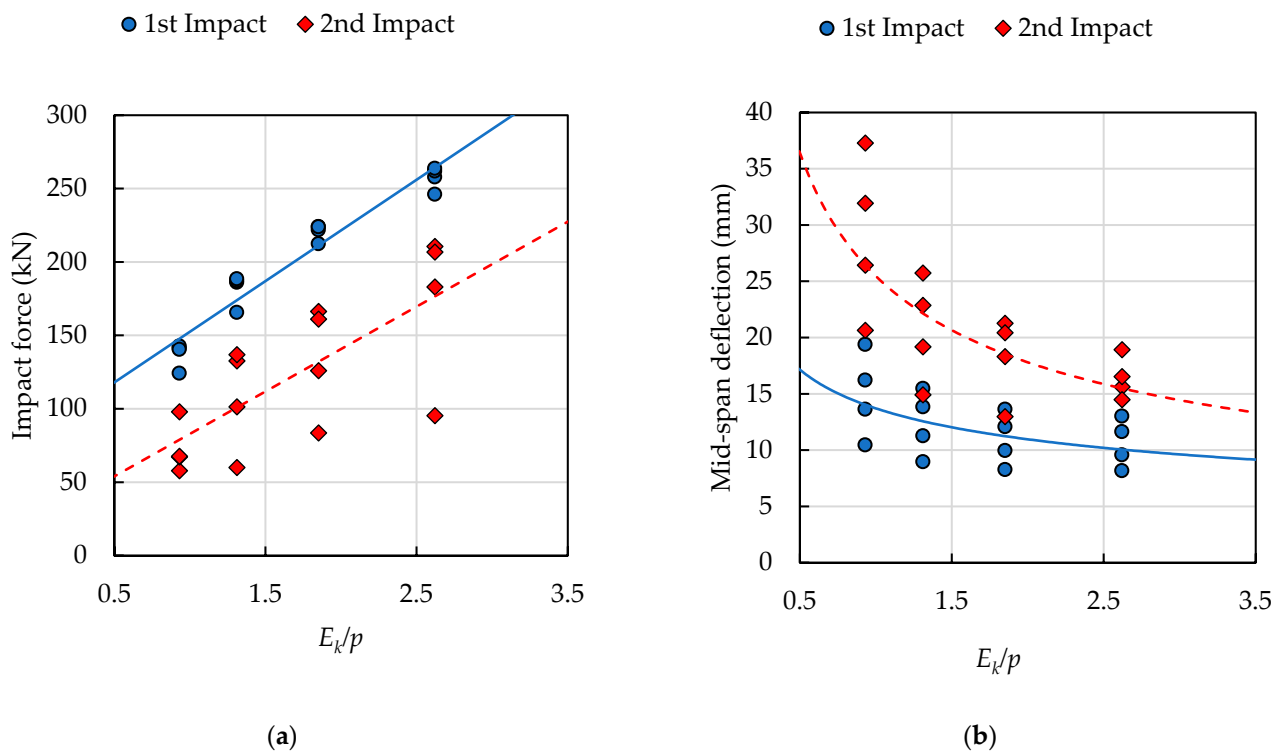


Figure 12. Relationship between the colliding index and: (a) impact force, (b) mid-span deflection.

3.7. Empirical Equation for Predict the Maximum Deflection of RC Member

Several researchers have proposed an empirical equation to predict the deflection of the RC member under impact loading using the method of least squares [8,22]. The level of the input kinetic energy was the main factor affecting the peak mid-span deflection of the RC members. There has been no equation considering the effect of the momentum. Tachibana et al. [22] proposed an empirical equation to predict the maximum midspan deflection of a simply supported RC beam with a span length of 1.0 to 2.0 m, as expressed in Equation (10). E_k is the input impact energy, and P_m is the total mean impact force calculated from the total impulse divided by the impact duration.

$$\delta_{\max} = 0.71 \frac{E_k}{P_m} \quad (10)$$

Using Equation (10), the mid-span deflections of the test specimens under the first impact were calculated and compared with the numerical results, as seen in Figure 13. It was found that the equation can be used to estimate the maximum deflection of the specimens under the dropped mass of 600 kg. However, the equation overestimates the mid-span deflection for the other specimens, which are subjected to the smaller dropped masses (300, 150, and 75 kg). This is because specimens under high colliding index tend to have shorter impact duration than those under low colliding index. This results in a significant decrease in the total mean impact force (P_m), which caused the equation to overestimate the midspan deflection for both the first and the second impacts, as shown in Figure 14. In addition, the predicted maximum deflection for the second impact of 600 kg dropped mass specimens (blue-square dot) from Equation (10) was overestimated by about 22%.

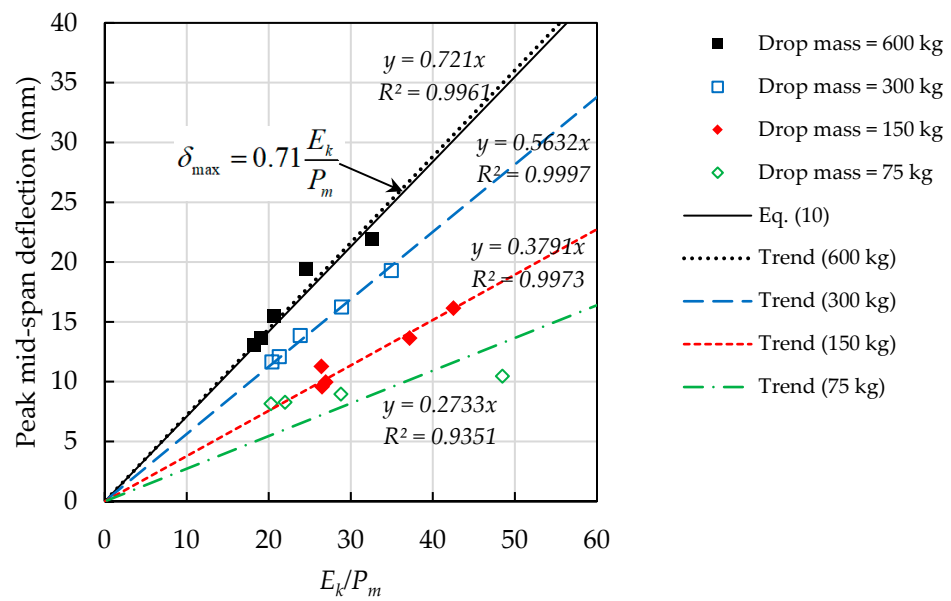


Figure 13. Relationship between deflection and impact energy to impact force ratio.

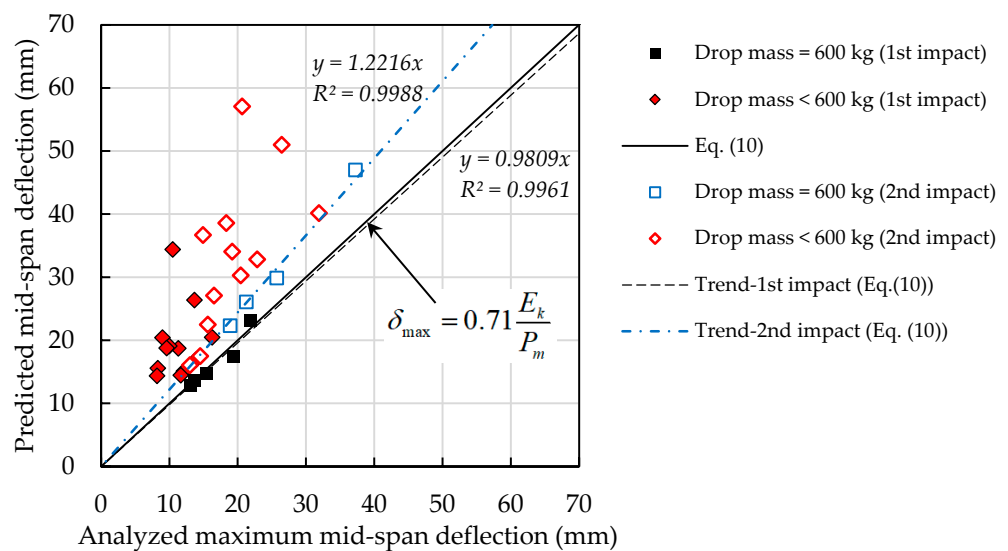


Figure 14. Analyzed maximum mid-span deflection against the predicted maximum mid-span deflection from Equation (10).

Based on the fact that the maximum mid-span deflection tends to decrease with the increasing colliding index, the effect of the colliding indexes should be taken into consideration. Equation (11) is a modified version of Equation (10), where the effect of the colliding index (*CI*) is included in the calculations. Since the colliding index is the ratio of the input impact energy and the momentum, Equation (11) can be re-expressed by Equation (12).

$$\delta_{\max} = \left(0.71 \frac{E_k}{P_m}\right) / CI \tag{11}$$

$$\delta_{\max} = 0.71 \frac{p}{P_m} \tag{12}$$

Figure 15 shows the predicted maximum mid-span deflection from Equation (12). It is seen that the modified equation is able to nicely predict the maximum mid-span deflection for the specimen with every dropped mass. Except for the second impact of specimens with a 600 kg dropped mass, Equation (12) was overestimated by 20–40%.

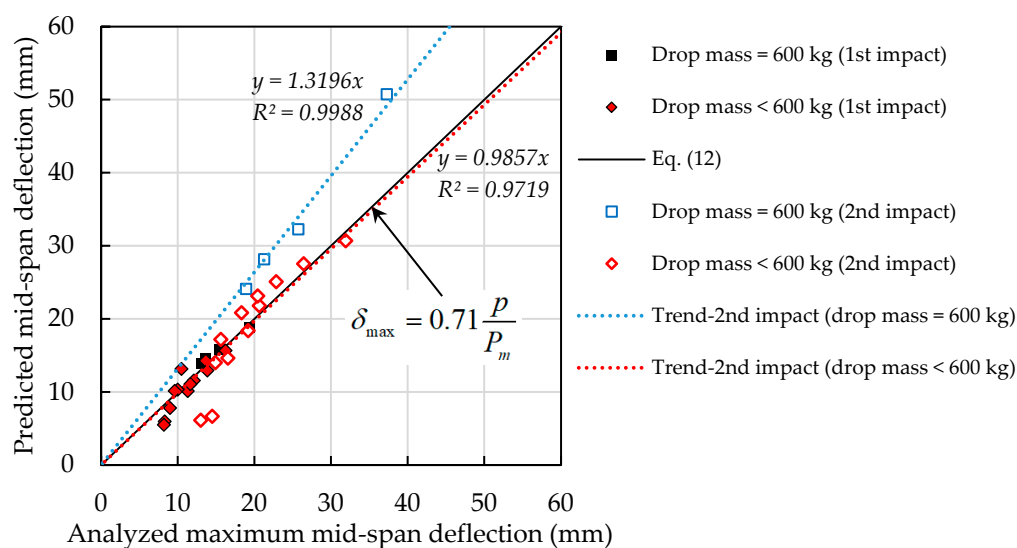


Figure 15. Analyzed maximum mid-span deflection against the predicted maximum mid-span deflection from Equation (12).

4. Conclusions

This study presented the numerical simulation of 16 RC columns subjected to double impact loadings at mid-span. The input impact energy was kept constant at 1029 J for both the first and second impacts. Different combinations of the impact velocity and dropped mass were selected, resulting in various impact momentums. The axial load ratios vary between 0.0, 0.1, 0.2, and 0.3 of the compressive strength of the concrete of the column's cross-section. The following conclusions can be drawn from the analytical results:

- Defining the damage and deflection from impact by using only the impact energy could be misleading due to the effect of impact momentum. Under the same level of the input impact energy, the different combinations of dropped mass and impact velocity create a difference in impact momentum, which results in a variation in the impact response of the RC column. Increasing impact momentum tends to increase the overall flexural damage and yields larger mid-span deflection but lowers the peak impact force. On the other hand, lower impact momentum yields more local damage with smaller mid-span deflection but higher peak impact force. In an extreme case where the impact momentum increases from 393 to 1112 kg·m/s, the peak mid-span deflection of the specimen without axial load increases by around 85%, while the peak impact force decreases by around 50%.
- Regardless of the inhibitory effect on flexural crack development of the influence of the axial load, increasing the axial load ratio above 0.2 of the concrete cross-sections led to a change in failure mode from flexural mode previously induced by the first impact to shear and crushing mode under the second impact. This is because the axial load contributes to the increase in flexural resistance and effectively maintains it throughout the first impact. However, the flexural damage due to the first impact reduced the shear transfer capacity of the concrete section, which led to shear failure. For practical design of structures under repeated impact loading, an additional shear reinforcement should be added to prevent sudden shear failure.
- The colliding index was used to clearly indicate the level of the collision based on the effect of the momentum under given kinetic energy. It is evidenced that the colliding index affects the behavior of the RC column under double impact loads, where the peak impact force increases proportionally to the increasing colliding index. The peak mid-span deflection decreases with the increasing colliding index.
- The newly proposed modified equation, which included the effect of the colliding index on the mid-span deflection, yielded a more accurate result in predicting the

maximum mid-span deflection of every specimen under equal energy but different momentum impact.

- In this study, the investigation was carried out to reveal the effect of impact momentum and axial load. In future studies, damage assessment, evaluation of the impact capacity of the damaged RC member, and the strengthening method shall be further researched.

Author Contributions: W.T.: analysis, writing original draft, review. C.H.: conceptualization, methodology, writing original draft, review, editing. S.L., H.Z., and V.V.: validation and review. All authors contributed to the article and approved the submitted version. All authors have read and agreed to the published version of the manuscript.

Funding: This research was funded by Thailand Science Research and Innovation (TSRI), under the Research and Researchers for Industries (RRI) scholarship, No. PHD59I0092, and PCC Post-Tension Co., Ltd. as a co-contributor, TRF Senior Research Scholar (RTA6280012).

Institutional Review Board Statement: Not applicable.

Informed Consent Statement: Not applicable.

Data Availability Statement: All datasets presented in this study are included in the article.

Conflicts of Interest: The authors declare no conflict of interest.

References

1. Hansapinyo, C.; Latcharote, P.; Limkatanyu, S. Seismic building damage prediction from GIS-based building data using artificial intelligence system. *Front. Built Environ.* **2020**, *6*, 576919. [[CrossRef](#)]
2. Ketsap, A.; Hansapinyo, C.; Kronprasert, N.; Limkatanyu, S. Uncertainty and Fuzzy Decisions in Earthquake Risk Evaluation of Buildings. *Eng. J.* **2019**, *23*, 89–105. [[CrossRef](#)]
3. Saicheur, K.; Hansapinyo, C. Seismic Loss Estimation and Reduction after Structural Rehabilitation in Chiang Rai City. *Walailak J. Sci. Technol.* **2017**, *14*, 485–499.
4. Saicheur, K.; Hansapinyo, C. Structural repair prioritization of buildings damaged after earthquake using fuzzy logic model. *J. Disaster Res.* **2016**, *11*, 559–565. [[CrossRef](#)]
5. Zhao, M.; Wu, G.; Wang, K. Comparative Analysis of Dynamic Response of Damaged Wharf Frame Structure under the Combined Action of Ship Collision Load and Other Static Loads. *Buildings* **2022**, *12*, 1131. [[CrossRef](#)]
6. Hansapinyo, C.; Wongmatar, P.; Vimonsatit, V.; Chen, W. Pounding of Seismically Designed Low-rise Reinforced Concrete Frames. *Proc. Inst. Civ. Eng. Struct. Build.* **2019**, *172*, 819–835. [[CrossRef](#)]
7. Wongmatar, P.; Hansapinyo, C.; Bi, K.; Vimonsatit, V. The effect of shear and bending capacities on impact behavior of RC beams. In Proceedings of the 24th Australian Conference on the Mechanics of Structures and Materials (ACMSM24), Perth, Australia, 6–9 December 2016; Taylor and Francis: Abingdon, UK, 2016; pp. 561–566.
8. Wongmatar, P.; Hansapinyo, C.; Vimonsatit, V.; Chen, W. Recommendations for Designing Reinforced Concrete Beams Against Low Velocity Impact Loads. *Int. J. Struct. Stab. Dyn.* **2018**, *18*, 1850104. [[CrossRef](#)]
9. Pham, T.M.; Hao, H. Plastic hinges and inertia forces in RC beams under impact loads. *Int. J. Impact. Eng.* **2017**, *103*, 1–11. [[CrossRef](#)]
10. Zhao, D.; Yi, W.; Kunnath, S.K. Shear mechanisms in reinforced concrete beams under impact loading. *J. Struct. Eng.* **2017**, *143*, 04017089. [[CrossRef](#)]
11. Saatic, S.; Vecchio, F.J. Effects of shear mechanisms on impact behavior of reinforced concrete beams. *ACI Struct. J.* **2009**, *106*, 78–86.
12. Ozbolt, J.; Sharma, A. Numerical simulation of reinforced concrete beams with different shear reinforcements under dynamic impact loads. *Int. J. Impact. Eng.* **2011**, *38*, 940–950. [[CrossRef](#)]
13. Magnusson, J.; Hallgren, M.; Ansell, A. Air-blast-loaded, high-strength concrete beams. Part I: Experimental investigation. *Mag. Concr. Res.* **2010**, *62*, 127–136. [[CrossRef](#)]
14. Jahami, A.; Tamsah, Y.; Khatib, J.; Baalbaki, O.; Kenai, S. The behavior of CFRP strengthened RC beams subjected to blast loading. *Mag. Civil. Eng.* **2021**, *103*, 10309.
15. Thilakarathna, H.M.I.; Thambiratnam, D.P.; Dhanasekar, M.; Perera, N. Numerical simulation of axially loaded concrete columns under transverse impact and vulnerability assessment. *Int. J. Impact. Eng.* **2010**, *37*, 1100–1112. [[CrossRef](#)]
16. Liu, B.; Fan, W.; Guo, W.; Chen, B.; Liu, R. Experimental investigation and improved FE modeling of axially-loaded circular RC columns under lateral impact loading. *Eng. Struct.* **2017**, *152*, 619–642. [[CrossRef](#)]
17. Gholipour, G.; Zhang, C.; Mousavi, A.A. Effects of axial load on nonlinear response of RC columns subjected to lateral impact load: Ship-pier collision. *Eng. Fail. Anal.* **2018**, *91*, 397–418. [[CrossRef](#)]
18. Hansapinyo, C.; Limkatanyu, S.; Zhang, H.; Imjai, T. Residual Strength of Reinforced Concrete Beams under Sequential Small Impact Loads. *Buildings* **2021**, *11*, 518. [[CrossRef](#)]

19. Jin, L.; Zhang, R.; Du, X.; Dou, G. Structural behavior of the steel fiber reinforced concrete beam under multiple impact loadings: An experimental investigation. *Int. J. Damage Mech.* **2019**, *29*, 503–526. [[CrossRef](#)]
20. Kishi, N.; Mikami, H.; Matsuoka, K.G.; Ando, T. Impact Behavior of Shear-Failure-Type RC Beams Without Shear Rebar. *Int. J. Impact Eng.* **2002**, *27*, 955–968. [[CrossRef](#)]
21. Fujikake, K.; Li, B.; Soeun, S. Impact response of reinforced concrete beam and its analytical evaluation. *J. Struct. Eng. ASCE* **2009**, *135*, 938–950.
22. Tachibana, S.; Masuya, H.; Nakamura, S. Performance based design of reinforced concrete beams under impact. *Nat. Hazards Earth Syst. Sci.* **2010**, *10*, 1069–1078. [[CrossRef](#)]
23. Tantrapongsaton, W.; Hansapinyo, C.; Wongmatar, P.; Limkatanyu, S.; Zhang, H.; Charatpangoon, B. Analysis of colliding index on impact behavior of RC columns under repeated impact loading. *Comput. Concr.* **2022**, *31*, 19–32.
24. Yu, Y.J.; Cho, J.Y. Analysis of Effect of Momentum on the Behavior of RC Beams Under Low Velocity Impact Loading. *Struct. Under Shock. Impact XV WIT Trans. Built Environ.* **2018**, *180*, 149–157.
25. Hwang, H.J.; Yang, F.; Zang, L.; Baek, J.W.; Ma, G. Effect of Impact Load on Splice Length of Reinforcing Bars. *Int. J. Concr. Struct. Mater.* **2020**, *14*, 40. [[CrossRef](#)]
26. Jin, L.; Lan, Y.; Zhang, R.; Du, X. Impact resistance of RC beams under different combinations of mass and velocity: Mesoscale numerical analysis. *Arch. Civ. Mech. Eng.* **2020**, *20*, 119. [[CrossRef](#)]
27. ACI 318–19. *Building Code Requirements for Reinforced Concrete and Commentary*; American Concrete Institute: Farmington Hills, MI, USA, 2019.
28. LS-DYNA. *LS-DYNA Keyword User's Manual*, Version 971; Livermore Software Technology Corporation: Livermore, CA, USA, 2007; Volume 1.
29. Hallquist, J.O. *LS-DYNA Theory Manual*; Livermore Software Technology Cooperation: Livermore, CA, USA, 2006.
30. Liu, G.R.; Quek, S.S. *The Finite Element Method*; Butterworth-Heinemann, Elsevier Science Ltd.: Oxford, UK, 2003.
31. Hughes, T.J.R.; Liu, W.K. Nonlinear finite element analysis of shells: Part II. Three-dimensional shells. *Comput. Methods Appl. Mech. Eng.* **1981**, *27*, 331–362. [[CrossRef](#)]
32. Hughes, T.J.R.; Liu, W.K. Nonlinear finite element analysis of shells: Part I. Two-dimensional shells. *Comput. Methods Appl. Mech. Eng.* **1981**, *27*, 167–181. [[CrossRef](#)]
33. Tantrapongsaton, W.; Hansapinyo, C. Impact response of reinforced concrete columns with different axial load under low-velocity impact loading. *Key Eng. Mater.* **2019**, *803*, 322–330. [[CrossRef](#)]
34. Tantrapongsaton, W.; Hansapinyo, C.; Wongmatar, P.; Chaisomphob, T. Flexural reinforced concrete members with minimum reinforcement under low-velocity impact load. *Int. J. GEOMATE* **2018**, *14*, 129–136. [[CrossRef](#)]
35. Malvar, L.J.; Ross, A.C. Review of strain rate effects for concrete in tension. *ACI Mater. J.* **1998**, *95*, 735–739.
36. CEB Bulletins. Concrete Structures under impact and impulsive loading. In *Comité Euro-International du Béton*; Bulletin d'Information: Lausanne, Switzerland, 1988.
37. Malvar, L.J. Review of static and dynamic properties of steel reinforcing bars. *ACI Mater. J.* **1998**, *95*, 609–616.
38. Johansson, A.; Fredberg, J. Structural Behaviour of Prestressed Concrete Beams during Impact Loading. Master's Thesis, Chalmers University of Technology, Gothenburg, Sweden, 2015.
39. Qin, F.; Pingan, W. Main factors affecting failure modes of blast loaded RC beams. *Chin. J. Comput. Mech.* **2003**, *1*, 39–42.
40. Ye, J.; Wang, Y.; Cai, J.; Chen, Q.; He, A. Evaluation of Residual Lateral Capacities of Impact-Damaged Reinforced Concrete Members. *Buildings* **2022**, *12*, 669. [[CrossRef](#)]